



1 Intercomparison of IAGOS-CORE, IAGOS-CARIBIC and 2 WMO/GAW-WCCOS Ozone Instruments at the Environmental 3 Simulation Facility at Jülich, Germany

4 Herman G.J. Smit¹, Torben Galle^{1,4}, Romain Blot², Florian Obersteiner³, Philippe Nédélec², Andreas
5 Zahn³, Jean-Marc Cousin², Ulrich Bundke¹, Andreas Petzold¹, Valerie Thouret², Hannah Clark²

6
7 ¹ Institute of Climate and Energy Systems: Troposphere (ICE-3), Forschungszentrum Jülich (FZJ), Jülich, Germany.

8 ² Laboratoire d'Aerologie, Université Toulouse III - Paul Sabatier, CNRS, Toulouse, France.

9 ³ Institute of Meteorology and Climate Research (IMK-ASF), Karlsruher Institut für Technologie (KIT), Karlsruhe, Germany.

10 ⁴ Previously published under the name Torben Blomel.

11
12 *Correspondence to:* Herman G.J. Smit (h.smit@fz-juelich.de)

13 **Abstract.** In the frame of the Quality Assurance (QA) plan of the In-service Aircraft for a Global Observation System
14 (IAGOS), IAGOS-CORE and IAGOS-CARIBIC UV-photometer instruments have been compared with the dual-beam UV-
15 Ozone (O₃) PhotoMeter (OPM) of the World Calibration Center of Ozone Sondes (WCCOS) at the Forschungszentrum
16 Jülich in an environmental simulation chamber. The WCCOS is established as part of the WMO-GAW measurement quality
17 program of the global ozonesonde network for more than 30 years, in which the OPM instrument serves as the ozone
18 reference standard. In the simulation chamber, pressure, temperature, and ozone concentration can be controlled at quasi-
19 realistic flight conditions between the Earth surface (~1000 hPa) and ~35 km altitude (5 hPa). During the intercomparison,
20 different ascent/descent and cruise altitude profiles of ozone, pressure and temperature have been simulated between the
21 surface and ~12 km altitude (200 hPa).

22 In general, the two O₃ instruments P1-O3 (IAGOS-CORE) and CAR-O3 (IAGOS-CARIBIC) showed good agreement with
23 the OPM reference standard within 5-6 %. At a pressure of 400-500 hPa the agreement was even within 2 %. The observed
24 differences are small but systematic and reproducible during this experiment. CAR-O3 showed a small, but pressure
25 independent deviation of -(1.5 - 2.5) % ± 1.5 % compared to the OPM. P1-O3 revealed O₃ deviation to the OPM which changes
26 with pressure of about +2% at 1000 hPa to -3% at 400 hPa, which might be an artefact on the experimental set-up and subject
27 for further investigations. This intercomparison is a first step of the long-term goal to get the global ozone sonde data (GAW-
28 NDACC-SHADOZ-GRUAN) and IAGOS-O3 (CORE: P1-O3, CARIBIC: CAR-O3) data traceable to one common reference,
29 the OPM instrument of WCCOS. Recommendations are given for further regular validation of the flown instruments on
30 external consistency in general and specifically towards the synergy of IAGOS-O3 and ozonesonde data.



31 1 Introduction

32 Ozone (O₃) is both chemically and radiatively one of the most important trace gases in the atmosphere. It forms the
33 stratospheric ozone layer shielding the Earth's surface from harmful UV sunlight (WMO/UNEP, 2023), while it is the major
34 precursor of the hydroxyl radical (OH), the principal chemical detergent controlling the oxidation capacity (e.g. Thompson et
35 al., 1992) and air quality in the troposphere (e.g. Cooper et al., 2014). Tropospheric ozone is also a potent natural and
36 anthropogenic greenhouse gas (IPCC, 2023). Monitoring the vertical ozone distribution on a regional as well as a global scale
37 is essential for understanding long-term changes in both tropospheric and stratospheric ozone, as each may be affected by
38 changes in the dynamics or chemistry of the atmosphere and its impact on life on Earth.

39 Beside of the traditional balloon borne ozonesonde network (Smit et al., 2021) to sample tropospheric ozone, in the 1990's
40 new ozone measuring platforms started their routine operations such as Lidar (e.g. McDermid et al., 1991; Ancellet et al.,
41 1998), FTIR (e.g. Schneider et al., 2005; Vigoroux et al., 2008) and the in-service aircraft programs of MOZAIC
42 (Measurement of OZone and water vapor by Airbus In-service airCRAFT) (Marenco et al., 1998a) and CARIBIC (Civil
43 Aircraft for the Regular Investigation of the atmosphere based on an Instrumented Container) (Brenninkmeijer et al., 1999) .
44 Both in-service aircraft programs have been joined since 2011 into the IAGOS (In-service Aircraft in a Global Observing
45 System) long term monitoring programme (<https://www.iagos.org>; Petzold et al., 2015) as part of the European Research
46 Infrastructure for global observations of atmospheric composition (Petzold et al., 2024). During normal scheduled flight
47 operation IAGOS measures in-situ ozone mixing ratios at cruise altitude (9-12 km) and during take-off and landing since
48 August 1994 and over more than 70,000 flights are archived in the IAGOS-database (<https://iagos.aeris-data.fr>). The data are
49 widely used for climatological and trends analysis (e.g. Petetin et al., 2016; Cohen et al., 2018; Gaudel et al., 2020; Wang et
50 al., 2022) as well as for model evaluations (e.g. Hu et al., 2017; Wagner et al., 2021).

51
52 Crucial for such long-term observations is to prove and monitor their long-term stability as well as the traceability of the
53 devices to a reference instrument on a regular basis. This can be done by checking the flown instruments on their internal and
54 external consistency. The internal consistency of the IAGOS ozone instruments and their long-term measurements have been
55 evaluated by Blot et al. (2021) and regular procedures have been developed to ensure the internal consistency over time.
56 External consistency checks have been done in the past through in-flight comparison with ozonesonde measurements within a
57 certain coincidence of space and time (Thouret et al., 1998; Staufer et al., 2013, 2014; Tanimoto et al., 2015; Tarasick et al.
58 2019; Wang et al., 2024). In general, over the entire period of more than 25 years of observations good agreement within 5-
59 10% between the observing platforms has been achieved, whereby the ozone sondes consistently tend to measure about 5%
60 more than the aircraft do.

61 In this study the external consistency of the IAGOS (CORE and CARIBIC) ozone UV photometer instrument has been
62 investigated through intercomparison with the ozone photometer (OPM) of the World Calibration Centre of Ozone Sondes
63 (WCCOS, <https://www.wccos-josie.org/en>) at the Forschungszentrum Jülich (FZJ) at their environmental simulation facility



64 to calibrate airborne ozone and water vapor sensors. The WCCOS is established as part of the WMO-GAW measurement
65 quality of the global ozonesonde network, whereby the OPM instrument serves as the ozone reference instrument. In the GAW-
66 WCCOS simulation chamber pressure, temperature, and ozone concentration can be controlled at quasi-realistic atmospheric
67 conditions varying between 1000 hPa (surface) and 5 hPa (upper stratosphere) (Smit et al., 2000). The IAGOS-CORE O₃
68 instrument (here called “P1-O3”) is part of the so-called IAGOS-CORE package P1 that is an EASA certified aeronautical
69 equipment. Several Package P1 units (14 units in 2024) are operated on commercial Airbus A340 and A330 aircraft (10 aircraft
70 of 8 international airlines in 2024). O₃ volume mixing ratio (VMR) measurements are performed for every flight from take-
71 off to landing (cruise legs at about 180-250hPa). The tested CARIBIC instrument (here called “CAR-O3”) is part of the
72 CARIBIC container laboratory and flown since 2010 on board an Airbus A340 by Lufthansa (Brenninkmeijer et al., 2007).
73 This intercomparison is a first step of the long-term goal to get the global ozone sonde data (GAW-NDACC-SHADOZ-
74 GRUAN) and IAGOS-O₃ (CORE: P1-O3 & CARIBIC: CAR-O3) data traceable to one common reference (OPM of WCCOS).
75

76 The key objective of the intercomparison is to investigate the performance of the three ozone UV-photometer instruments
77 (OPM, P1-O₃, CAR-O₃) under controlled laboratory conditions in the ESC, thereby, simulating typical flight conditions of
78 atmospheric pressure, temperature and ozone concentration between the surface and cruise altitude (Z=10-12.5 km). During
79 the intercomparison different ascent/descent and cruise altitude profiles of ozone have been simulated. This paper presents and
80 discusses the major results of the observed performance of the different instruments in quantitative terms. An outlook will be
81 given on how to have ozone measurements of IAGOS and ozonesondes both traceable to one common ozone reference
82 instrument, i.e. the OPM of the WCCOS chamber.

83 2. Experimental Details

84 2.1 Ozone UV-Photometer Instruments of IAGOS and WCCOS

85 The principle of the three UV-ozone photometer instruments involved in the intercomparison are based on the spectroscopic
86 UV-absorption measurement of ozone at a wavelength around 254 nm in a well-defined sample chamber according to Beer-
87 Lambert absorption law:

$$88 \quad \ln\left(\frac{I_t}{I_0}\right) = -L \cdot \sigma_{O_3} \cdot C_{O_3} \quad (1)$$

89 where I_0 (= zero mode) and I_t (=sample mode) are the lamp intensities at the detector when the chamber contains the sampled
90 gas with and without removal of the ozone, respectively. L is the length of the absorption chamber, σ_{O_3} is the molecular
91 absorption cross section of ozone at a wavelength of about 254 nm, and C_{O_3} is the average concentration of ozone in the
92 absorption chamber. Since L and σ_{O_3} are well known quantities, and the transmittance $R_t = I_t/I_0$ of the absorption chamber is
93 determined by the ratio of the two observed signal intensities of the photo detectors in sample and zero mode, respectively,



94 then the ozone concentration C_{O_3} can be derived (Eq.1). Through additional measurement of the pressure P_C and temperature
95 T_C inside the absorption chamber the volume mixing ratio of ozone μ_{O_3} can be derived from C_{O_3} .

$$96 \quad \mu_{O_3} = -\frac{k}{L \cdot \sigma_{O_3}} \cdot \frac{T_C}{P_C} \cdot \text{Ln} \left(\frac{I_t}{I_0} \right) \quad (2)$$

97 whereby k is the Boltzmann constant

98

99 All instruments use the same widely applied UV-absorption cross-section ($\sigma_{O_3} = (1,147 \pm 0.024) \times 10^{-17} \text{ cm}^2 \text{ molecule}^{-1}$)
100 determined by Hearn (1961). In 2025 a new cross-section ($\sigma_{O_3} = (1,1329 \pm 0.0035) \times 10^{-17} \text{ cm}^2 \text{ molecule}^{-1}$: CCQM.O3.2019 (
101 <https://www.bipm.org/en/gas-metrology/ozone>), by Hodges et al., 2019) will be introduced in the global ozone ground-based
102 monitoring networks (CCQM-GAWG, 2024) which is about 1.29 % lower, however, this will have no impact on the results
103 of the present intercomparison.

104 All three ozone instruments are dual-beam UV-photometers that have two identical UV-absorption chambers (cuvettes), each
105 alternating between reference mode (ozone-free air generated by directing it through an ozone scrubber being CuO/MnO₂) and
106 sample mode. A valve assembly alternates the scrubbed air between the two chambers, such that one chamber is in null mode
107 while the other chamber is in sample mode or vice versa. The mode alternation compensates for changes in the light
108 transmission through the cuvettes (e.g. due to temperature driven mechanical changes or changes of the reflectivity of the
109 cuvettes due to changing surface coatings) and finally doubles the measurement frequency. Although the principle of operation
110 is similar for all three photometer types, the instrumental layouts have significant differences. Specifications of the P1-O₃,
111 CAR-O₃ and OPM ozone UV-photometer instruments participating in the intercomparison are summarised in Table 1. In
112 general, the overall instrumental relative uncertainty is predominantly determined by the uncertainty of σ_{O_3} , the molecular
113 absorption cross-section of ozone. For in-situ atmospheric measurements, however, the sampling uncertainty must be
114 considered too, which is also dependent on the design of the air sampling (use of pump in inlet line or not), the use of proper
115 material (e.g. PTFE) to avoid ozone losses at the walls, the thermal concept and the electronic design. Therefore, regular pre-
116 and post-flight tests and characterization of the instruments are essential.

117 **2.1.1 GAW-WCCOS Ozone Photometer (OPM)**

118 The dual-beam UV-absorption ozone photometer (OPM) of the WCCOS serves as reference. It was developed by Proffitt and
119 McLaughlin (1983) for use on stratospheric balloons. The overall uncertainty is ± 2 % at P=1000-10 hPa. The instrument serves
120 as reference (standard) of the GAW global ozonesonde network. The OPM is enclosed in a Styrofoam box, mounted inside a
121 cylindrical vacuum tank which is connected to the simulation chamber and thus operates at the same pressure level as inside



122 the simulation chamber. Details of the instrument and the data processing, including uncertainty budget are described in Proffitt
123 and McLaughlin (1983).

124 It is to be mentioned that no ozone reference instrument running at reduced pressures exists at any NMI (National Metrological
125 Institute) in the world. This means that before and after the intercomparison, the OPM could only be compared at laboratory
126 pressure conditions (1000 hPa) with a commercial, NIST-traceable “surface” ozone UV photometer of Thermo Electron
127 Instruments (Model TEI-49) at volume mixing ratios between 0 and 200 ppbv. The agreement was within ± 1 ppbv below 100
128 ppbv and $\pm 1\%$ above. No systematic bias was observed. Validation of the performance of the OPM at reduced pressures could
129 only be done based on the evaluation of the measured physical parameters of the OPM as described in Proffitt and McLaughlin
130 (1983).

131 **2.1.2 IAGOS-CORE Ozone Instrument (P1-O3)**

132 The ozone monitor P1-O3 in IAGOS-CORE is a modified dual beam UV-photometer of Thermo Scientific (Model 49i)
133 integrated together with a CO-infrared monitor in a special aeronautic flight box (Nédélec et al., 2015). The P1-O3 monitor
134 measures ozone at cabin air pressure conditions. Hereby, one UV-absorption cell is in measuring-mode and the second cell is
135 in zero-mode. In zero mode the ozone is removed from the sampled air by an ozone scrubber (MnO_2 -catalyst filter) before
136 the air sample enters the cell that is in zero-mode. Alternating, every 4 seconds (3 s for air flushing the cells and 1s for the
137 measurement), the cells are switched from sample into zero-mode and vice versa. The pressure and temperature in the
138 absorption cells are measured to derive the ozone volume mixing ratio from the measured amount of light absorbed by ozone
139 using Beer’s absorption law.

140 In-flight ambient air is sampled through a forward-facing pitot tube and thereafter compressed by the Pump Box up to cabin
141 air pressure and then led into the manifold at the inlet of P1-O3 splitting the total air flow into the nominal sample flow of 4
142 vol-l/min required for the O_3 and CO monitors and an excess flow, respectively. Thereby, the excess air flow is continuously
143 monitored to ensure that the minimum required volume-flow of Pump Box (25 vol-l/min at ground, 5 vol-l/min at cruise
144 altitude) is obtained. To avoid any losses of ozone due to physical and chemical interactions on the walls of the sampling
145 lines, the pitot inlet tube and the interior of the pumps of the Pump Box are coated with PTFE, while all tubings are made of
146 PTFE too.

147 Before and after aircraft operation (or each ~ 6 months, respectively), each P1-O₃-instrument is checked (without the Pump
148 Box) against a Thermo Scientific model 49PS reference instrument at several concentration levels to prove the instrument
149 that its linearity is within 1 %. In addition, each P1-O3 instrument is sent once a year to the French Laboratoire National
150 d’Essais (LNE) for comparison with a traceable National Institute of Standards and Technology (NIST). The overall
151 uncertainty is better than ± 2 ppbv $\pm 2\%$ above. (Nédélec et al., 2015).



152 Each flown Package P1s (P1-O3 plus Pump Box) for IAGOS-CORE are compared before and after flight periods with the
153 same MOZAIC-Rack as standard since the beginning of the program. Therefore, it is possible to remove systematic biases
154 in the long-term time series and the resulting measurement uncertainty should represent only the contribution from random
155 errors (Blot et al, 2021). More details of Package IAGOS-P1 (Pump Box and P1-O3 instrument) and its operation are given
156 by Nédélec et al. (2015) and Blot et al. (2021).

157 **2.1.3. IAGOS-CARIBIC Ozone Instrument (CAR-O3)**

158 The IAGOS-CARIBIC (CAR-O3) UV-photometer ozone instrument is fully custom-made and likewise applies a dual beam
159 configuration. In zero-mode the ozone is removed using a MnO₂-scrubber controlled at 38°C for maximum efficiency of
160 100%. Two three-way valves toggle each 4s to guide sample air and zero air alternatively between the two sample cuvettes.
161 Each measurement takes 2 s and is preceded by flushing the cells for 2 s.

162 In contrast to commercial ozone monitors, the instrument uses a UV-LED (Seti, TUD59H1B) as light source (see section 2.1
163 of Zahn, 2016). The LED light is guided into the two sample cuvettes (to ~47% each) using a beam-splitter. The remaining 6
164 % is measured by the opposing reference diode to actively control the LED (further stabilized at 20°C using a Peltier-
165 element) to constant light emission with an uncertainty of ~10⁻⁴ (which is not possible with the conventionally used low-
166 pressure Hg discharge lamps). However, since the UV-LED emission spectrum has a full-width half-mean (FWHM) of ~11
167 nm and may age, it is initially calibrated against a reference UV photometer and thereafter regularly cross-checked (about
168 every 3 months).

169 Two photodiodes (Hamamatsu S1226) at the end of the cuvettes measure the UV light intensity using a two-channel (not
170 multiplexing) 24-bit sigma-delta amplifier. Temperature is measured on the outside and the inside of the cuvettes. Pressure is
171 measured directly at the exhaust of the cuvettes. Sample flow during aircraft operation of CAR-O3 is determined by the
172 RAM-pressure through the CARIBIC inlet system. This guarantees a minimum flow of 1.5 vol-l/min at cruise altitude.
173 During the experiments reported here (without the RAM pressure on aircraft), a flow of ~2 vol-l/min was enforced by a
174 pump downstream of the instrument in combination with a needle valve for manual control of the flow. The main
175 specifications are listed in Table 1. Further details of handling and data processing are described in Zahn (2016) as well as
176 Obersteiner (2024, <https://doi.org/10.5281/zenodo.11104076>).

177 The measured precision (1-sigma) is 0.06 ppb at 1000 hPa and the response time of 4s. A simple calculation based on the
178 photon flux reaching the photodiodes (inferred from its photosensitivity and the measured photo current) and the detected
179 photo current noise indicate that this precision exactly agrees (to within 10-15 %) with the measured shot noise, that is,
180 CAR-O3 is quantum-noise limited and higher precision can only be reached with a stronger UV-LED or a longer absorption
181 (cuvette) length.



182 The total uncertainty of 2 ppb or 2% (whatever is higher) is dominated by the uncertainty of the O₃ cross section around 255
 183 nm (Zahn, 2016). CAR-O₃ is regularly (typically each 3-4 months) compared in the laboratory with a working standard and
 184 once a year with a 2.7 m long-path UV photometer (by UMEG).

185

186 **Table 1. Specifications of the P1-O₃, CAR-O₃ and OPM ozone UV-photometer instruments participating in the**
 187 **intercomparison.**

188

Property	P1-O ₃ IAGOS-CORE	CAR-O ₃ IAGOS-CARIBIC	OPM GAW-WCCOS
Light Source	Hg-Lamp (254 nm)	UV-LED (near 254 nm)	Hg-Lamp (254 nm)
UV Abs. Length	38 cm	38 cm	40 cm
Pressure	Cabin air	Ambient air	Ambient air
Inlet	Pitot (forward) + Compressor	Pitot (forward) + RAM-pressure	N/A
Sample Volume Flowrate	24 l _v /min (4 l _v /min for P1-O ₃ & P1-CO)	2 l _v /min	8 l _v /min
Response Time	4 seconds	4 seconds	2 seconds
Precision <100 ppbv >100 ppbv	± 1 ppbv ± 1 %	± 0.1 ppbv ± 0.1 %	± 1 ppbv ± 1 %
Overall Uncertainty <100 ppbv >100 ppbv	± 2 ppbv ± 2 %	± 2 ppbv ± 2 %	± 2 ppbv ± 2 %
Reference	Nédélec et al., 2015	Zahn, 2016	Proffitt and McLaughlin, 1983

189

190 **2.2. Environmental Simulation Facility: GAW-WCCOS**

191 **2.2.1 GAW-WCCOS Simulation Chamber**

192 The GAW-WCCOS simulation chamber established at the Forschungszentrum Jülich (FZJ) is designed to investigate the
 193 performance of different types of balloon-borne ozone sensors as well as airborne humidity sensors to measure the vertical
 194 distribution of atmospheric ozone and water vapor, respectively (Smit et al., 2000). The key component of the facility is a
 195 simulation chamber with a test room volume of about 500 liters (80x80x80 cm) whose pressure as well as temperature can be
 196 dynamically regulated between 5 and 1000 hPa and between 200 and 300 K at temperature rates between -2K/min and
 197 +5K/min. The volume mixing ratio of ozone can be dynamically regulated between 5 and 10000 ppbv to simulate typical



198 atmospheric ozone levels between the surface and 35 km altitude. Since 1994, the facility has been established as the World
199 Calibration Centre for Ozone Sondes (WCCOS) as part of the QA/QC-management plan of the Global Atmosphere Watch
200 (GAW) program of the World Meteorological Organization (WMO). In the scope of this framework since 1996, international
201 JOSIE (Jülich Ozone Sonde Intercomparison Experiment) campaigns have been conducted to assess the performance of the
202 major types of ozone sondes used within the global network of ozone sounding stations (Smit et al., 2007, 2024; Thompson et
203 al., 2019). The dual beam UV-photometer OPM (section 2.1.1) serves thereby as an ozone reference. The entire simulation
204 process is automated by computer control to guarantee reproducible ambient conditions. JOSIE observations have
205 demonstrated that the experimental set-up of the WCCOS simulation chamber experiment has a reproducibility of about $\pm 1\%$.
206 Details of the facility and its use as WCCOS are given by Smit et al. (2000).

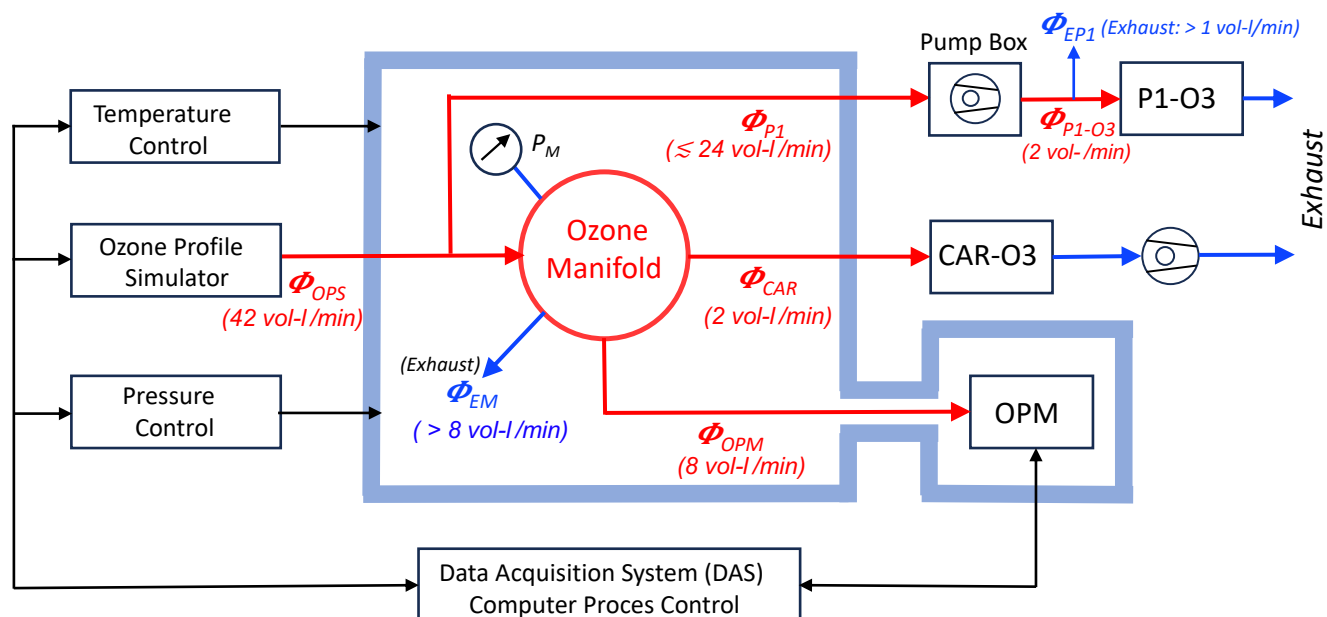
207 **2.2.2 Ozone Profile Simulator (OPS)**

208 The Ozone Profile Simulator (OPS) unit of GAW-WCCOS (Smit et al., 2000) is used to simulate reproducible pressure
209 dependent ozone profiles dynamically in time. Therefore, a separate gas mixing system is installed to provide up to four ozone
210 sensors plus the UV-photometer (OPM) with pre-set ozone concentrations. Ozone is photolytically generated by UV-
211 irradiation in a zero-grade airflow through a quartz glass (Suprasil) tube using a low-pressure Hg-discharge lamp. Via the
212 photodissociation of oxygen molecules at a wavelength of 185 nm ozone is formed at high levels of 0.1-0.2 % at a constant
213 flow of 50 cm³/min through the quartz glass cell (pressurized at 4000 hPa, volume: ~ 40 cm³). To vary the ozone volume
214 mixing ratio between 10 and 10000 ppbv at different air pressures, the high-ozone airflow is dynamically diluted by a two-
215 staged mixing with zero-grade air flows. All air flows are regulated by mass-flow controllers (Smit et al., 2000). The air used
216 is dried and purified such that any sensitivities of the UV-Photometers to humidity or sudden changes of it (Wilson and Birks,
217 2006) can be excluded. The sample flow is connected to a glass manifold inside the simulation chamber to feed the different
218 O₃-instruments, whereby excess air can flow via an exhaust, such that the inlet tubes of all connected instruments are at the
219 same pressure condition as inside the WCCOS-chamber.

220 **2.3 Experimental Design Intercomparison**

221 **2.3.1 Experimental Setup**

222 The schematic of the experimental setup is shown in Figure 1. Ozone-containing air is produced in the OPS and fed into a gas
223 manifold located inside the simulation chamber. The inlet tubes of the three ozone instruments are connected to the manifold
224 via gas-feed through (all made of PTFE). For CAR-O3 it's simply a 2 m tube (ID = 4 mm), while for P1-O3 the inlet line goes
225 via the P1-Pump Box that compresses the sample air to cabin or (here) laboratory pressure before entering the P1-O3
226 instrument. The OPM, mounted in a vacuum tank connected to the simulation chamber, is at the same pressure condition as
227 inside the chamber.



228

229 **Figure 1: Schematics of the experimental setup for the intercomparison at the WCCOS, showing the ESC with OPM of the WCCOS,**
 230 **the connection to the IAGOS-CORE and IAGOS-CARIBIC ozone instruments, the ozone manifold located inside the simulation**
 231 **chamber and its control systems, including the computer-controlled DAS.**

232 The sample manifold consists of a spherical glass vessel with a volume of about 150 cm³ with radially arranged connections
 233 to the individual ozone instruments with the inlet of the simulated ozone air flow Φ_{OPS} being in the centre of the manifold.
 234 Excess air is exhausted via an additional tube such that the manifold is kept to the sample volume pressure (measured by a
 235 pressure sensor) and to prevent the inlet lines of the ozone instruments from overpressure effects that may cause measurement
 236 artefacts.

237 For the JOSIE experiments (for testing ozone sondes), the volume flow rate of the simulated ozone air flow Φ_{OPS} is kept
 238 constant at 12 vol-l/min which is sufficient to provide four ozone sondes (maximum 4 x 0.25 vol-l/min) and the OPM
 239 (maximum 8 vol-l/min). For the IAGOS-ozone intercomparison, higher flow rates were required, see instrument sample flows
 240 in Table 1. The total volume flow rate is at least 36 vol-l/min. To ensure a significant exhaust flow at the manifold, we thus
 241 increased the typical volume flow of 12 vol-l/min by an additional 30 vol-l/min flow controller to obtain a total volume flow
 242 Φ_{OPS} of 42 vol-l/min and thus an exhaust flow of the manifold of 6 vol-l/min (Fig.1). The pressure P_M inside the manifold had
 243 been monitored to ensure to keep it a few hPa higher than the pressure in the test chamber itself to avoid any leakage effects
 244 of air from the chamber into the manifold. The P1-O3 sample flow we had to branch off from the ozone profile simulator flow
 245 before entering the manifold (Fig.1), because it was shown that the high sampling volume rate of P1-O3 pump box would
 246 otherwise cause leakage effects when P1-O3 had been directly connected with a Teflon fitting at the inlet glas tube of the
 247 manifold.



248 2.3.2 Simulation of Realistic Flight Conditions

249 It is essential to operate the chamber at appropriate pressure conditions to simulate realistic flight conditions that the IAGOS
250 instruments experience when connected to the air inlets. Both air-sample inlets (of IAGOS-CORE and IAGOS-CARIBIC) are
251 facing forwards and thus use the RAM (dynamic) pressure generated by the high speed of the aircraft, whereby on IAGOS-
252 CARIBIC a special inlet configuration hinders (aerosol and cloud) particles larger than $\sim 2 \mu\text{m}$ to enter the sampling line. At
253 the maximum cruise altitude of about 12.5 km the lowest static air pressure is 180 hPa at a typical aircraft speed of Mach =
254 0.81 ± 0.02 causing an adiabatic compression factor of about 1.6. This leads to a dynamic (RAM) pressure of about 100 hPa
255 and thus to a lowest total air pressure inside the inlets of about 280 hPa. Some pressure loss in the sampling results in minimum
256 pressure at the instrument air inlets of ~ 250 hPa. Note however, as P1-O3 runs a pump to compress sampled air to cabin
257 pressure (here laboratory pressure) before entering P1-O3 instrument, the pressure ranges of P1-O3 and CAR-O3 covered by
258 our tests are different, but for both instruments spans the relevant pressure ranges between surface and cruise altitude.

259 A. IAGOS-CORE = P1-O3

260 The P1-Pump Box supplied with sample air from the forward-facing inlet system compresses the sampled air to cabin air
261 pressure. The cabin air pressure is prescribed by civil aviation regulations to be above 750 hPa and usually ranges at 800-850
262 hPa at cruising altitude. In-flight, the maximum pressure difference between cabin and the inlet of P1-PU thus is $850 - 280 =$
263 570 hPa. For the present laboratory intercomparison we thus must cover the pressure range between 1000 hPa and 430 hPa (=
264 $1000 - 570$ hPa).

265 B. IAGOS-CARIBIC = CAR-O3

266 The CAR-O3 instrument doesn't use a pump, and its inlet pressure is the ambient static pressure, plus the RAM pressure minus
267 some pressure loss in the sampling line (see above), that is, 250 hPa at maximum cruise altitude. To simulate the RAM pressure
268 effect (exhaust at 180 hPa), during this laboratory intercomparison the CAR-O3 uses a pump at the exhaust to force an air flow
269 of about 2 vol-l/min (Fig.1).

270

271 3 Results

272 3.1. Introduction

273 Table 2 gives an overview of the simulation experiments performed. The first day (12 June 2023) was reserved for installation
274 of the equipment and for a short test run to ensure proper functioning of equipment and data acquisition of the different
275 instruments. On the second day (13 June 2023) another test of the P1-O3 and CAR-O3 instruments followed by sampling
276 outside ambient air. The results of these two tests are beyond the scope of this report. The core of the intercomparison itself



279 took place on 13 until 15 June 2023 with the four simulation experiments number 3 to 7, which will be presented here in more
 280 detail.

281

282 **Table 2. List of intercomparison experiments performed during the IAGOS-WCCOS Ozone Intercomparison (IWOI) campaign**
 283 **between 12 and 15 June 2023 at WCCOS (FZJ/IEK-8, Jülich, Germany).**

Date	Exp. Nr & Sim. Nr	Profile Type	UTC-Time	Pressure (hPa)	Remarks
Day#1: 12-06-2023	#1 & 223	Test	13:00-15:00	1000-300	Installation and testing equipment
Day#2.1: 13-06-2023	#2 & NAN	Ambient Air (Day2.1_Ambient)	07:30-09:30	1000	P1-O3 & CAR-O3 & No OPM
Day#2.2: 13-06-2023	#3 & 224	Ascent_CruiseDescent (Day2.2_Profile)	12:00-17:00	1000-400-400-1000	P1-O3 & CAR-O3 & OPM
Day#3.1: 14-06-2023	#4 & 225	Ascent_Cruise_Descent (Day3.1_Profile) Cruise: O3 Step-Up/Down	07:30-11:30	1000-400-400-1000	P1-O3 & CAR-O3 & OPM
Day#3.2: 14-06-2023	#5 & 226	Discrete Pressure Levels (Day3.2_Profile) Total OPS-Flow: 12 vol-l/min	11:30-14:00	1000-400-250	CAR-O3 & OPM & No P1-O3
Day#3.3: 14-06-2023	#6 & 226	Ascent-profile (Day3.3_Profile) Ascent Zero Ozone	14:00-15:00	1000-250	CAR-O3 & OPM & No P1-O3
Day#4.1: 15-06-2023	#7 & 228	Discrete Pressure Levels (Day3.3_Profile)	07:00-10:30	1000-400	P1-O3 & CAR-O3 & OPM

284

285 **3.2 Comparison of P1-O3, CAR-O3 and OPM at a pressure of 400-1000 hPa**

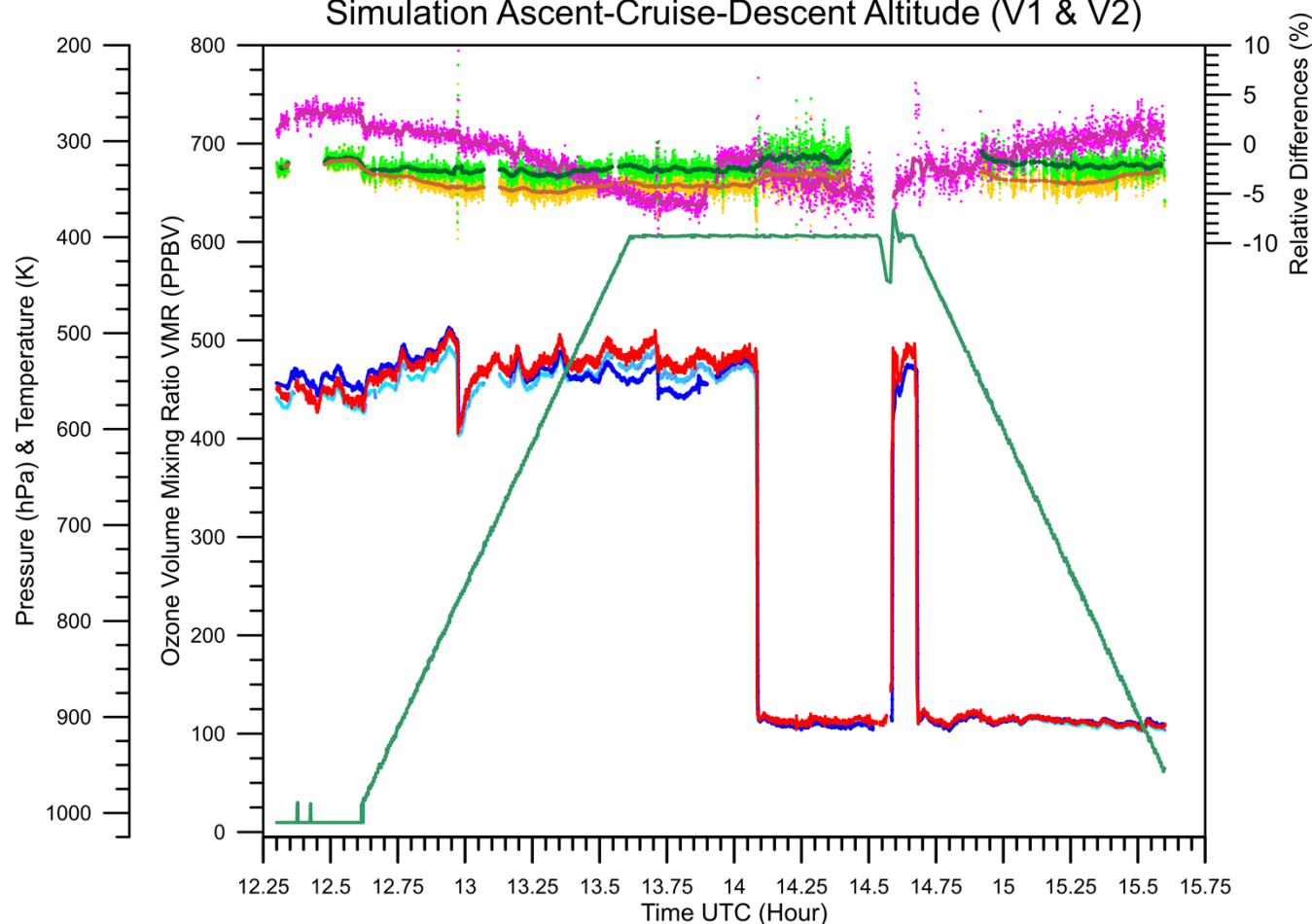
286 **3.2.1 Experiment #3: Ascent-Cruise-Descent**

287 Experiment #3 (numbering, see second column in Table 2) simulates an aircraft doing an “ascent - cruise altitude - descent”
 288 profile of pressure and ozone volume mixing ratio (Figure 2, 4, 5). The lowest pressure of 400 hPa is to simulate the maximum
 289 pressure difference the P1 pump box must achieve between cruise altitude and about 1000 hPa in the laboratory (see
 290 explanation in section 2.3.2.). In the first part of the simulation, during the ascent and the beginning part of the cruise phase,
 291 the ozone level was maintained at 400-500 ppbv to clean the inlet tubes of the OPM, P1-O3 (including P1-Pump Box) and
 292 CAR-O3 instruments. In the second part, the ozone was lowered to about 100 ppbv.

293



IAGOS O3-Comparison (IOC) 2023 - Exp#3: Simulation Ascent-Cruise-Descent Altitude (V1 & V2)



294

295

Figure 2: Experiment #3: Time-series of pressure (dark green) and ozone volume mixing ratio to simulate an ascent-cruise-descent track of an IAGOS aircraft for P1-O3 (blue), CAR-O3 (light blue) and OPM (red). The relative differences compared to each other are P1-O3 to OPM (magenta) and CAR-O3 (original: V1) to OPM (yellow) and CAR-O3 (pressure-sensor corrected: V2, see text) to OPM (light green). Fat solid lines are 3-minute running averages of the relative differences.

299

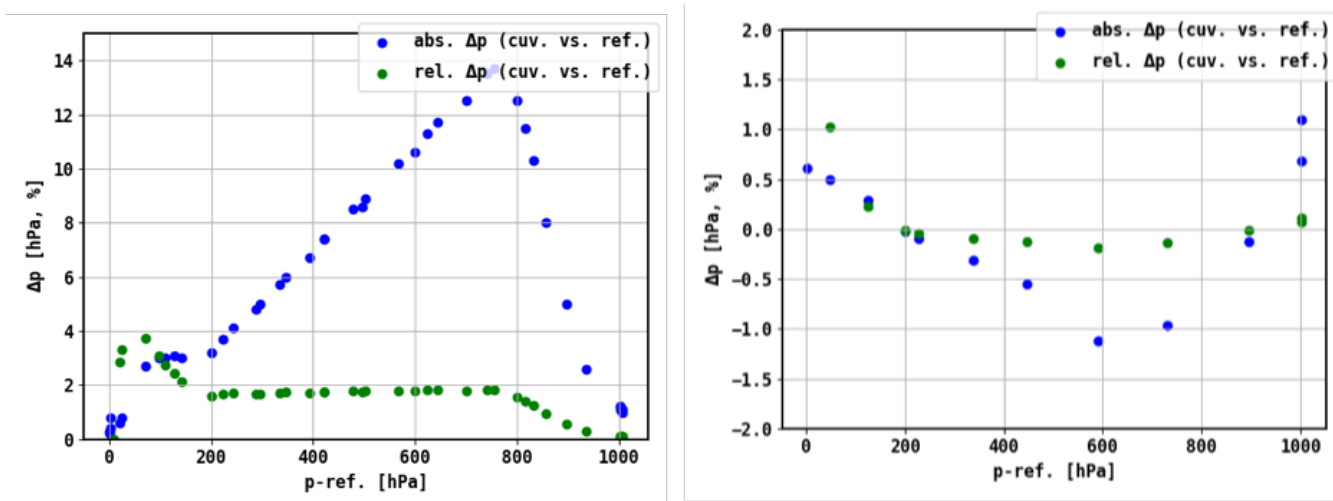
300

In general, the three instruments follow the simulated ozone profile well and agree among each other between -5 and +2% (Fig. 2). P1-O3 compared to the OPM shows a pressure dependence, that is, from +3% at 1000 hPa down to -5 % at cruise altitude conditions. The CAR-O3 instrument initially showed an increasing negative offset relative to the OPM of a 1% at 1000 hPa (at ~12:30) to -4 % at 800 hPa and lower pressures. This somewhat strange behaviour was subject to further investigations on the underlying cause. Indeed, in a subsequent test (May 2024), KIT found an issue with the electronic analog-digital converter of the data acquisition card of CAR-O3 that generated a systematic 2.2% difference of the pressure reading below a pressure of ~800 hPa (see Figure 3). This electronic artefact has been eliminated and the pressure readings before and

306

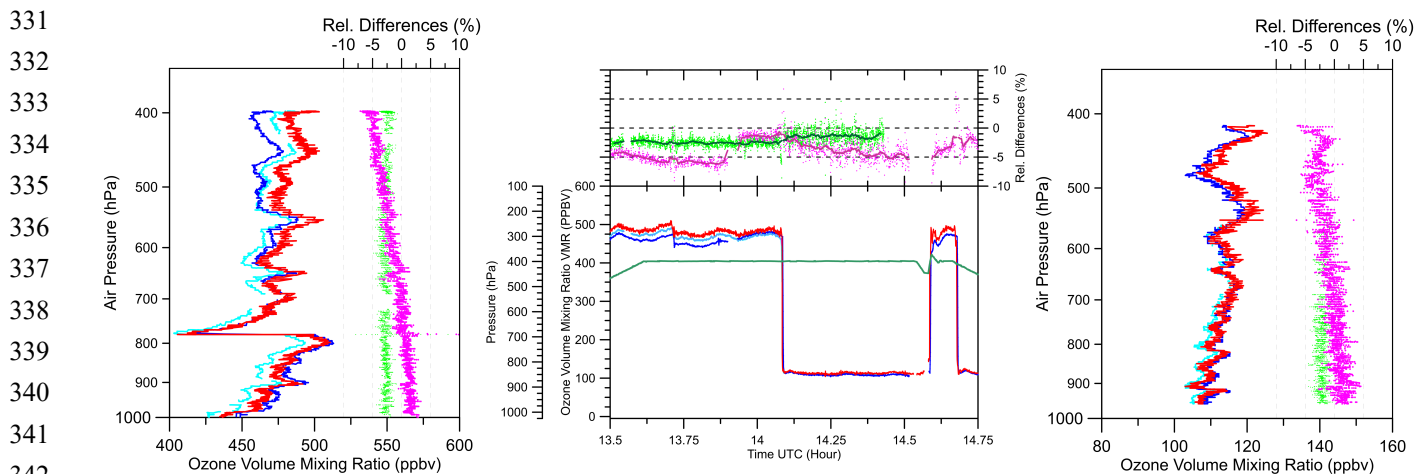


307 after the repairment of the AD-converter were compared against an accurate pressure sensor (Omega HHP360, accuracy: 0.25
 308 hPa). The observed pressure differences as function of pressure (Figure 3) are used to correct all original CAR-O3 data (version
 309 V1) into the new pressure-sensor corrected CAR-O3 data (version V2). After the correction the V2 data show a rather constant,
 310 pressure independent, deviation of about -2 % compared to the OPM. In this paper we only will present from now on the
 311 pressure corrected CAR-O3 data. Meanwhile, all CARIBIC-Ozone data in the IAGOS database (<https://iagos.aeris-data.fr/>)
 312 have been corrected accordingly.
 313



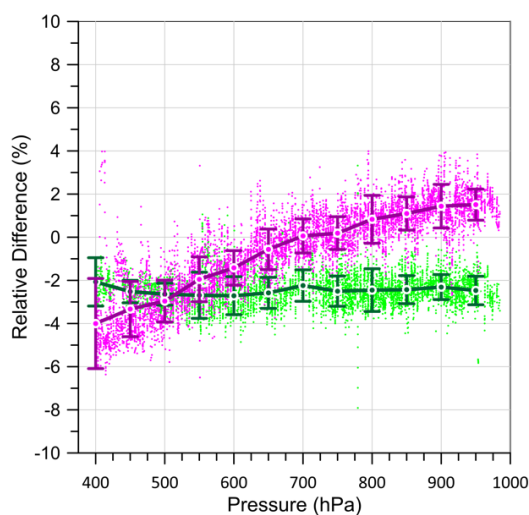
314
 315 **Figure 3 Comparison of CAR-O3 air pressure sensor (inside UV-absorption cuvette) against accurate pressure sensor (Omega,**
 316 **HHP360, uncertainty: 0.25 hPa) before (left diagram) and after (right diagram) solving the electronic artifact of the AD-converter**
 317 **(details see main text). Displayed are the pressure differences in hPa (blue dots) and their relative differences in % (green dots).**
 318

319 In Figure 4 the identical data (experiment No. 3, see Fig. 2) have been split into the vertical O₃-profiles during ascent (Fig. 4a)
 320 and descent (Fig. 4c) and the section at 400 hPa. The behaviour of P1-O3 and CAR-O3 described above occurs identically
 321 during ascent and descent and no indication for any hysteresis effects could be observed. This is also confirmed by the fast
 322 responses of both instruments on the sharp upward or downward steps of the simulated ozone levels.
 323
 324
 325
 326
 327
 328
 329
 330



343
344 **Figure 4. Experiment No. 3: Same data (and colours) as in Figure 2 but has been split into ascent (a: left diagram), cruise altitude**
345 **(b: center diagram) and descent (c: right diagram). The measured ascent and descent profiles are displayed as ozone versus the**
346 **simulated pressure (¹⁰Log scale), while the cruise track part is plotted as time series.**

347
348



349
350
351 **Figure 5. Experiment No. 3: Same data (and colours) as in Fig. 2, but relative differences among P1-O₃, CAR-O₃ and OPM as**
352 **function of pressure. Thick solid lines are averages over 50 hPa pressure bins with their 1 σ -standard deviation.**

353

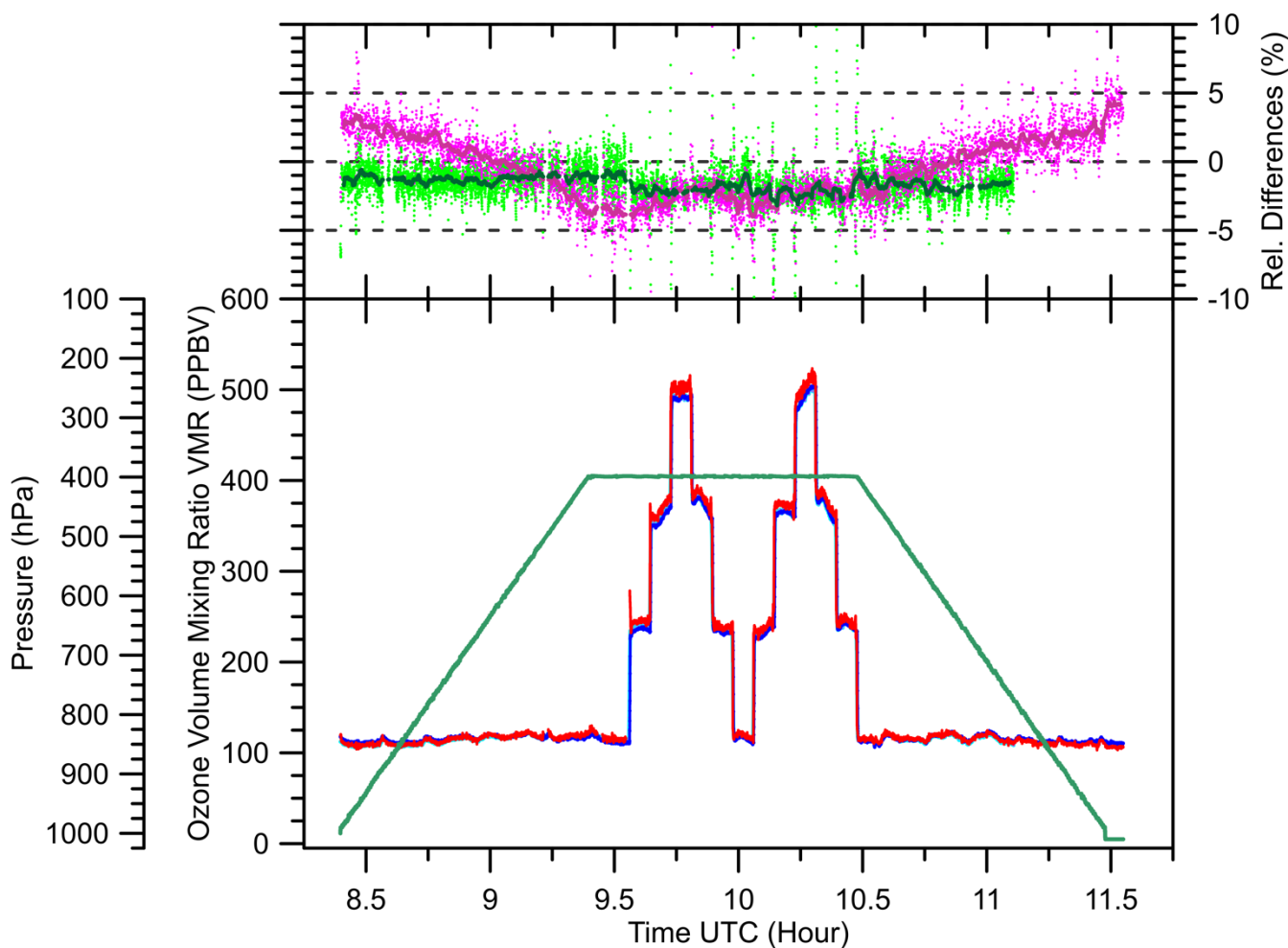


354 The results of this Exp#3 are summarized in Figure 5 that displays the relative differences of P1-O₃ and CAR-O₃ compared
355 to the OPM as scatter plot and function of the air pressure inside the chamber. The thick curves are the corresponding averages
356 over 50 hPa bins with their one standard deviation.

357 3.2.2 Experiment #4: Ascent - Cruise (O₃ steps) - Descent

358 This simulation experiment is similar to Exp. No. 3, with the following differences: during ascent and descent the ozone
359 volume mixing ratio was held at 110 ppbv, while at cruise altitude, the ozone was varied (stepped up and down) at different
360 levels of 100, 250, 370 and 500 ppbv, see Figures 6 - 8 equivalent to the Figures 2, 4 and 5 respectively.

361

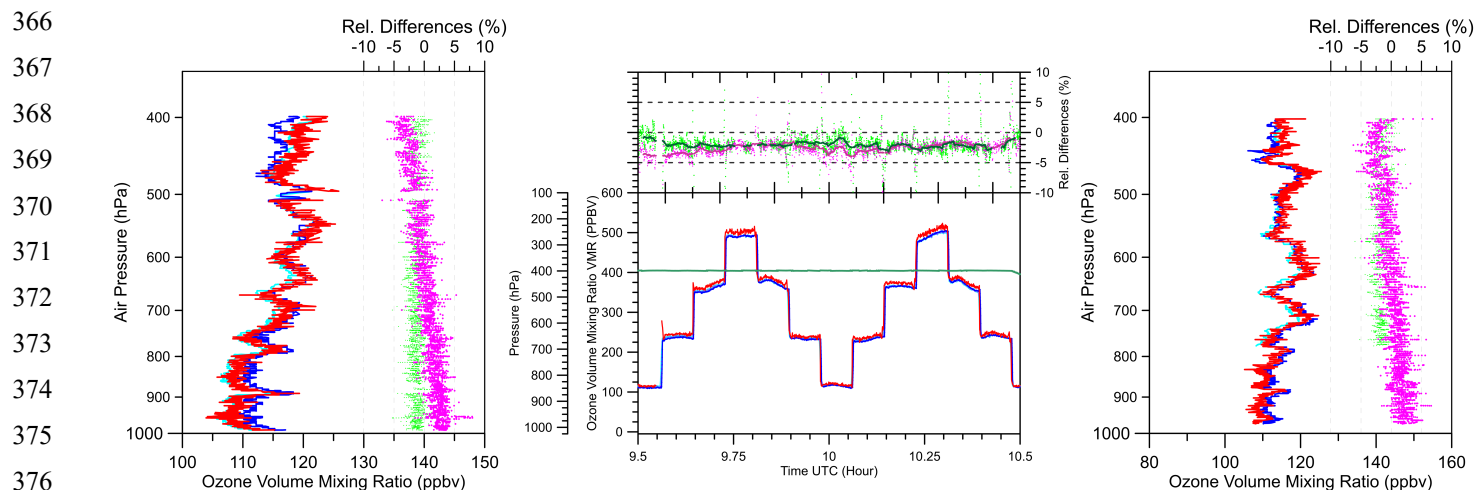


362

363 **Figure 6.** Experiment No. 4: Graph and colour coding identical to Fig. 2.

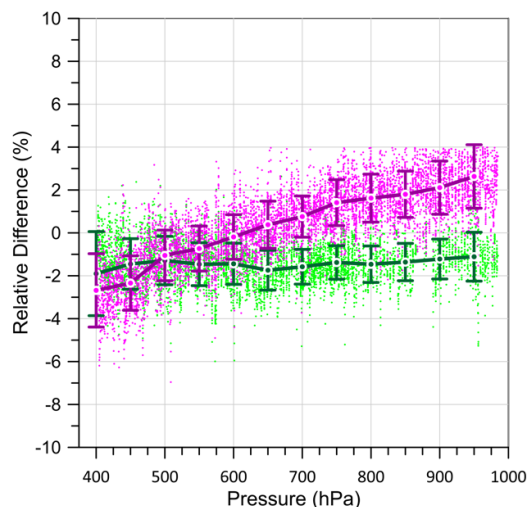
364

365



377 **Figure 7. Experiment No. 4: Graphs and colour coding identical to Fig. 4.**

378
 379 Also, in this simulation experiment the instruments follow the simulated ozone profile well and agree among each other
 380 between -3 and +3%. From Fig. 7 and 8 it is depicted that the P1-O3 compared to the OPM show a significant decrease with
 381 decreasing pressure, similar as in the previous Exp. No. 3 from +3% at 1000 hPa down to -3 % at 400 hPa (cruise altitude
 382 conditions). The CAR-O3 instrument relative to the OPM revealed a similar behaviour as in Exp. No. 3: - (1.5 – 2) % deviation
 383 that is constant at pressures between 1000 hPa and 400 hPa. Remarkable is that the span and slope of all data are identical to
 384 Exp. #3, but all data are shifted to (0.8 - 1.0) % higher values. Based on this observation we estimate the reproducibility of the
 385 experimental set-up within +/- 1%. Further, no indications are found on any memory or hysteresis effects for both instruments.
 386



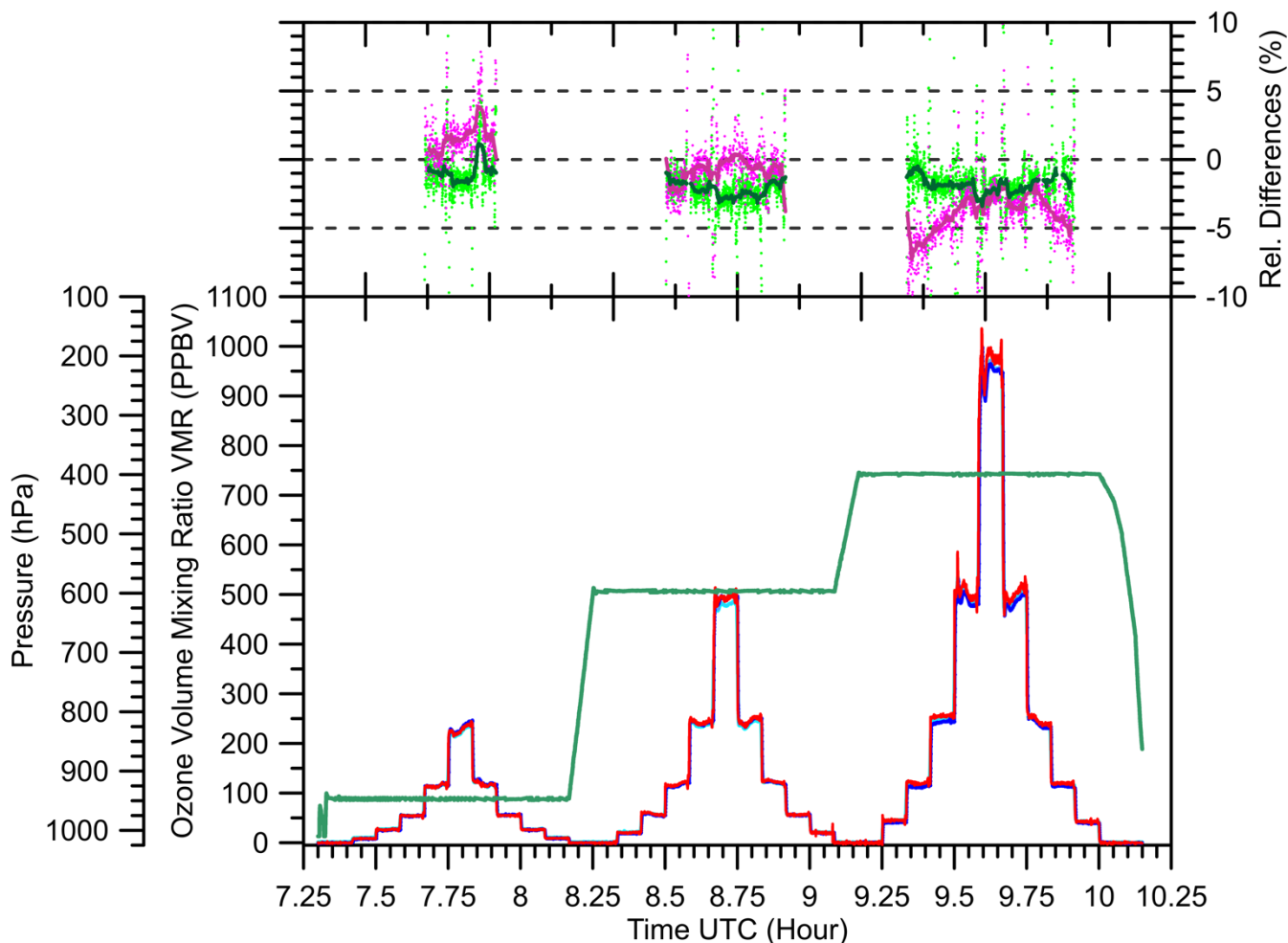
389 **Figure 8. Experiment No 4: Graph and colour coding identical to Fig. 5.**



390 **3.2.3. Experiment No. 7: O₃ Step Up/Down at Different Pressure Levels**

391 In this simulation experiment at three different discrete pressure levels (950, 600 and 400 hPa) the ozone levels were varied
 392 (step up and down) at discrete values representative for the corresponding pressure levels, (See Figures 9 and 10).

393



394

395 **Figure 9. Experiment #7: colour coding as listed in Figure 4.**

396

397 At low pressure around 400 hPa (Fig. 9), P1-O3 shows a small ozone dependent bias to the OPM from -5 % at ~100 ppbv to -
 398 2% at ~1000 ppbv. The bias of CAR-O3 relative to OPM is again (as in Exp#3 and #4) with -(1-2) % constant over the entire
 399 pressure range of 400 - 1000 hPa and ozone volume mixing ratios up to 1000 ppbv. Although the three instruments follow the
 400 even small ozone levels of below 100 ppbv only relative differences are shown in Fig. 9 for the higher levels. To compare the
 401 behaviour of P1-O3 and CAR-O3 in more detail, also at lower ozone levels, the instruments have been compared in Figure 10



402 with the three ozone VMR scatter plots of P1-O3 versus OPM and CAR-O3 versus OPM, respectively, for the three discrete
 403 pressure levels of 950, 600 and 400 hPa.

404

405

406

407

408

409

410

411

412

413

414

415

416

417

418

419

420

421

422

423

424

425

426

427

428

429

430

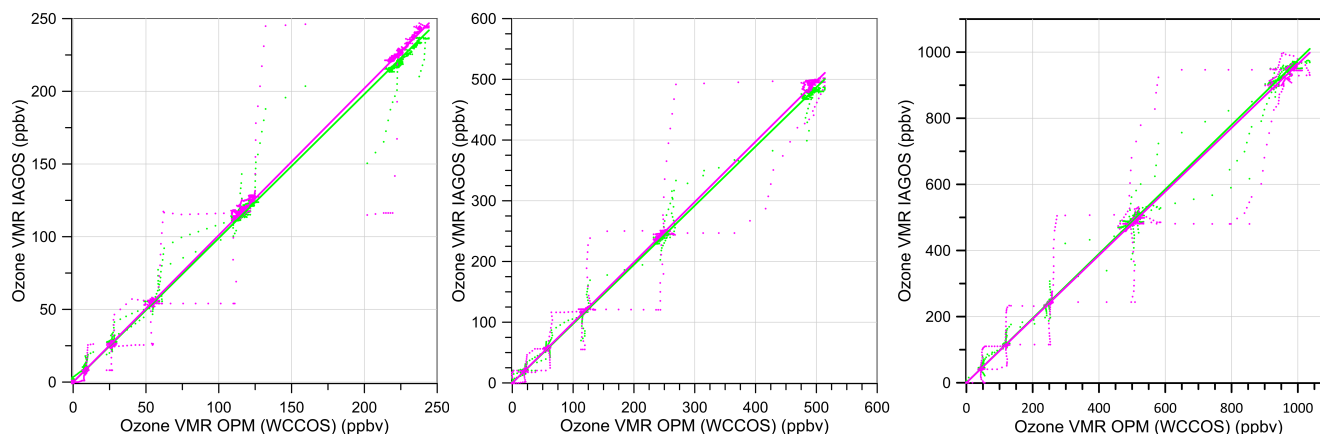


Figure 10. Experiment #7: Ozone pressures measured by IAGOS instruments versus OPM at different ozone VMR levels (ppbv) for three discrete constant air pressure levels: 950, 600 and 400 hPa. Displayed are the scatter plots of P1-O3 versus OPM (Magenta) and CAR-O3 versus OPM (Green) and the solid straight lines are their linear fits through the origin.

At each pressure level the slope of a linear curve fit through the origin of the scatter plots of P1-O3 and CAR-O3 versus OPM (Fig. 9) have been derived, while the offsets of the instruments have been determined in the periods when measuring zero ozone air by averaging over 5 minutes intervals (Fig. 8). The results for each pressure level (950, 600 and 400 hPa) are summarized in Table 3 for the entire ozone VMR range and for the lower ozone VMR levels which are more representative for tropospheric conditions.

This behaviour between the three instruments observed at ozone levels larger than about 100 ppbv is consistent with the results obtained from the Exp. #3 and Exp. #4. However, the small ozone dependent differences (P1-O3/OPM: $-(1-2)\%$ and CAR-O3/OPM: $+(1-2)\%$) observed at lower ozone pressures is not really understood but are still within the experimental reproducibility of about $\pm 1\%$ as mentioned in Section 3.2.2.



431 **Table 3. Offsets of OPM, P1-O3 and CAR-O3 determined from zero air measurements (Fig.8) and slope of linear curve fits through**
 432 **the origin of P1-O3 and CAR-O3 versus OPM scatter plots (Fig.9), respectively, at three different air pressure levels: 950, 600 and**
 433 **400 hPa.**
 434

Pressure (hPa)	O3-Range (ppbv)	OPM Offset (ppbv)	P1-O3 Offset (ppbv)	CAR-O3 Offset (ppbv)	P1-O3/OPM Slope	CAR-O3/OPM Slope
950	0-250	-0.25±0.5	-0.30±0.6	1.5±0.2	1.01	0.99
950	0-100	--	--	--	0.99	1.01
600	0-600	-0.27±0.7	-0.08±0.3	1.5±0.3	0.99	0.99
600	0-150	--	--	--	0.98	1.00
400	0-1100	-0.13±1.2	-0.28±0.45	1.0±0.4	0.964	0.98
400	0-200	-0.38±1.0	-0.55±0.75	1.1±0.5	0.942	1.00

435

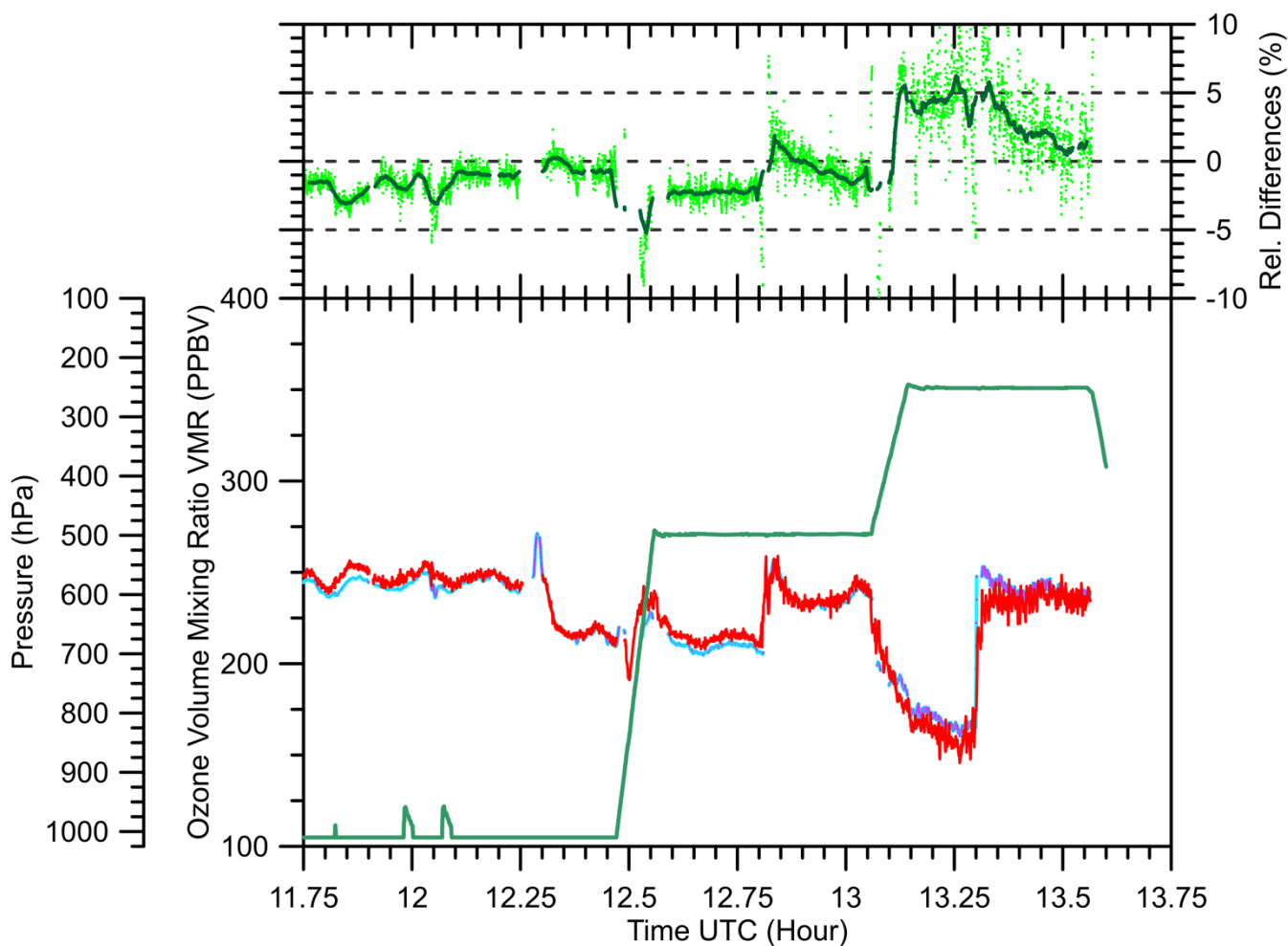
436

437 **3.3 Comparison CAR-O3 Versus OPM at 250-1000 hPa Pressure**

438 **3.3.1 Experiment #5: Discrete Pressure Levels (1000-250 hPa)**

439 To simulate the real cruise altitude conditions for CAR-O3 (see section 2.3.2), a simulation experiment was repeated at three
 440 different pressure levels (1000, 500 and 250 hPa), whereby the ozone volume mixing ratios were kept at levels between 150
 441 and 250 ppbv. The P1-O3 did not participate in this comparison experiment because the low-pressure level of 250 hPa is not
 442 within the specification of the P1-Pump Box to operate against 1000 hPa laboratory pressure instead of 850 hPa cabin air.
 443 pressure under real flight conditions (see section 2.3.2). In this simulation the total volume flow rate of the OPS, Φ_{OPS} is
 444 reduced to 12 vol-l/min. The results are shown in Figure 11.

445 At 1000 hPa and 500 hPa the results are very similar with the results of Exp.#3 and Exp. #4, while at 250 hPa initially CAR-
 446 O3 shows slight enhanced values of about + (4-5) % compared to OPM, but after about 10 minutes declined to + (1-2) %. The
 447 cause of this behaviour has been investigated by evaluating the housekeeping data of both instruments (CAR-O3 and OPM)
 448 as well as the OPS and ESC, however, no indication of any mal function of any of the components could be detected. Although
 449 the cause is not understood until now, it is subject for further detailed investigations.



450

451 **Figure 11. Experiment #5: colour coding as listed in Figure 9.**

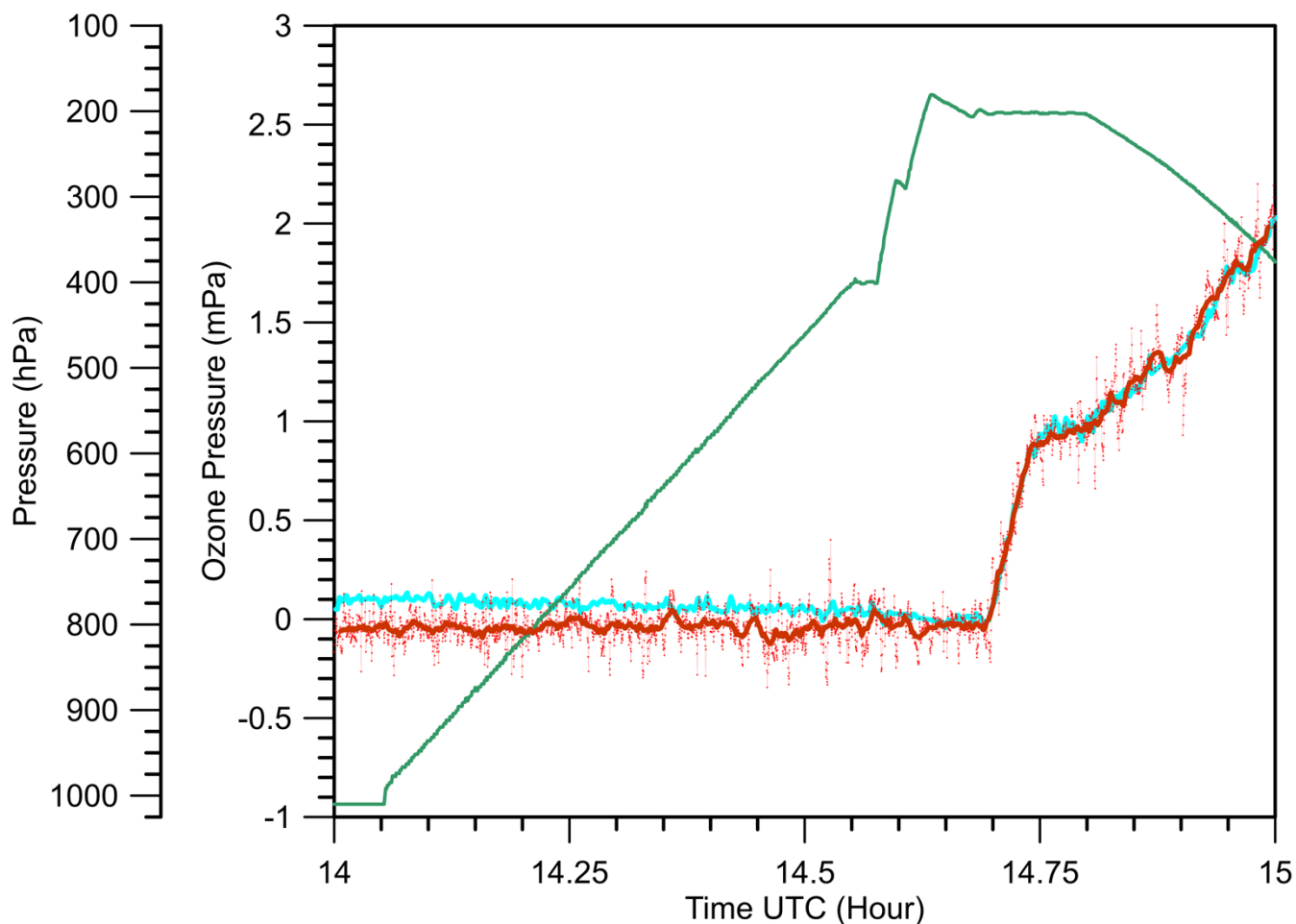
452 **3.3.2 Experiment #6: Zero O3 Ascent (1000-180 hPa)**

453 In this experiment the ascent pressure (down to 200 hPa) was simulated while ozone was kept at zero to measure the zero
 454 signals of the CAR-O3 and OPM, while P1-O3 did not participate in the experiment. The OPM showed a small negative offset
 455 about - (0.05 – 0.10 mPa), but a rather noisy signal, unrealistic high and most likely due to too high temperatures of the
 456 electronics of the instrument. The CAR-O3 showed a small positive offset of 0.1 mPa at 1000 hPa that vanishes towards lower
 457 pressures, which agrees with results of Exp.#7 (Table 3).

458

459

460



461

462

463

Figure 12. Experiment #6: Time series of pressure (green) and ozone pressure (mPa) for CAR-O3 (light blue) and OPM (red), while ozone is kept initially at zero and after 14.70 (~14:42) ozone increased towards 2 mPa.

464

4. Discussion, Conclusions and Recommendations

465

466

467

468

469

470

471

472

In general, the IAGOS-O₃ instruments P1-O₃ and CAR-O₃ as well as the OPM showed consistent and good agreement among each other within a range better than about 5 %. CAR-O₃ showed on average about -(1-2) % deviation to the OPM, but no clear pressure dependence within the 1000 hPa down to 400 hPa range, while at 250 hPa CAR-O₃ showed about 2-4 % more ozone than the OPM. P1-O₃ showed a good performance with a moderate increasing pressure dependent O₃ deviation to the OPM of about +2% at 1000 hPa to -3% at 400 hPa. The observed differences are small but systematic. The underlying causes should be better understood, also with respect to how far the observed results are consistent among the suite of instruments flown within IAGOS. Further, an experimental artefact of a few percent cannot be fully excluded, because we had to modify the WCCOS-JOSIE experimental setup to be able to adapt to the large sampling volume flow rate



473 of about 24 lv/min of the P1-O₃ (Section 2.3.1). However, no indications are found on any memory or hysteresis effects for
474 both instruments. For IAGOS-O₃ the long-term stability of the base line of the measured ozone records is extremely
475 important to derive long term ozone changes of the order of one percent per decade.

476
477 Further, the intercomparison experiments here have shown that the reproducibility of the performance of the OPM used here
478 as a standard, in combination with the experimental set up, is about within ± 1 %. It is to be noted that only for O₃-UV
479 photometer measuring at Earth surface conditions, a primary standard exists (at the Bureau International des Poids et
480 Mesures (BIPM), Paris, France), but not for the free atmosphere or at reduced pressure, respectively. Therefore, even all
481 intercomparisons in the past like JOSIE (comparison of ozonesondes against OPM) as well as this study (IAGOS-O₃ versus
482 OPM) must be interpreted as being relative to each other. Hereby in this intercomparison the OPM acts as the common
483 instrument to refer to.

484
485 This intercomparison is a first step with the goal to get the global ozone sonde data (GAW-NDACC-SHADOZ-GRUAN)
486 and IAGOS-O₃ (CORE & CARIBIC) data traceable to one common reference (OPM of WCCOS). While the aircraft and
487 sonde measurements are often complementary, but their records do not typically cover the same period. It is therefore
488 essential to know and quantify potential biases and characteristics over time when merging their long-term records for
489 process or trend studies. Tarasick et al. (2019) has evaluated earlier in-flight comparisons with ozonesonde measurements
490 within a certain coincidence of space and time (Thouret et al., 1998; Stauffer et al., 2013, 2014; Tanimoto et al., 2015) and
491 found a consistent average relative positive bias of 5 % - 10 % between the ozonesondes and IAGOS. In a most recent study
492 (Wang et al., 2024) has confirmed and discussed this observed bias, but no conclusive explanation could be given. It is
493 known that ozone sondes in the troposphere can overestimate ozone by up to 5% (Smit et al., 2007, 2024; Thompson et al.,
494 2019), while aircraft measurements may underestimate ozone due to wall losses when compressing the sampled air before
495 measurement (Dias-Lalcaca et al., 1998; Brunner et al., 2001; Schnadt-Poberaj et al., 2007). However, this intercomparison
496 study has shown that a freshly serviced Pump Box compressing the sampled air to cabin air pressure conditions, before
497 entering the P1-O₃ monitor unit of P1-CORE-package, has only a small to no impact of less than 2-3% compared to the total
498 measurement error. Further investigations on the performance of the Pump Boxes are needed, particularly the ones which
499 has been flown during long periods of IAGOS-CORE flight operation and thus may have been exposed to highly polluted air
500 masses containing contaminants (e.g. aerosols) near airports during take-off or landing of the aircraft. A key question thereby
501 is: Can these contaminants have an impact on the performance of P1-O₃ or may the self-cleansing effect through high ozone
502 concentrations, when flying in the stratosphere, be that efficient that the impact is small or can be neglected?

503 A more regular validation of IAGOS-O₃ on external consistency is therefore essential, which could be achieved by regular
504 comparisons of the IAGOS-O₃ instruments together with ozonesondes against the OPM of the WCCOS in their
505 environmental simulation chamber. This would be an important milestone in ozone research in the free troposphere and
506 UTLS.



507 **Acknowledgement**

508 The WCCOS has been sponsored by the Forschungszentrum Jülich GmbH and WMO-GAW. IAGOS is supported by the
509 European Commission, Airbus and the airlines (Deutsche Lufthansa, Air France, Austrian Airlines, Air Namibia, Cathay
510 Pacific, Iberia, China Airlines, Hawaiian Airlines, and Air Canada so far) that have carried the MOZAIC or IAGOS equipment
511 and performed the maintenance since 1994. IAGOS has been funded by the European Union projects IAGOS-DS and IAGOS-
512 ERI. Additionally, IAGOS has been funded by INSU-CNRS (France), Météo-France, Université Paul Sabatier
513 (Toulouse, France) and Forschungszentrum Jülich GmbH. The IAGOS database is supported in France by AERIS
514 (<https://www.aeris-data.fr>).

515 **Competing interests**

516 One of the co-authors Andreas Zahn is a member of the editorial board of Atmospheric Measurement Techniques.
517 The authors have no other competing interests to declare.

518 **List of Acronyms**

519	ASOPOS	Assessment of Standard Operating Procedures for OzoneSondes
520	CARIBIC	Civil Aircraft for the Regular Investigation of the atmosphere Based on an
521		Instrument Container
522	CCQM-GAWG	Consultative Committee for Amount of Substance: Metrology in Chemistry and Biology-
523		Gas Analysis Working Group
524	CO	Carbon monoxide
525	DS	Design Study
526	ECC	Electrochemical Concentration Cell
527	ERI	European Research Infrastructure
528	ESC	Environmental Simulation Chamber
529	FTIR	Fourier Transform Infra-Red spectroscopy
530	FZJ	ForschungsZentrum Jülich
531	GAW	Global Atmosphere Watch
532	GCOS	Global Climate Observing System
533	GRUAN	GCOS Reference Upper Air Network
534	IAGOS	In-service Aircraft for a Global Observing System
535	INSU	Institut National des Sciences de l'Univers
536	IPCC	Intergovernmental Panel on Climate Change



537	JOSIE	Jülich OzoneSonde Intercomparison Experiment
538	LIDAR	Laser Imaging Detection and Ranging
539	MOZAIC	Measurement of OZone and water vapor by Airbus in-service airCRAFT (now IAGOS)
540	NDACC	Network for the Detection of Atmospheric Composition Change
541	OPM	Ozone PhotoMeter Instrument (used as UV-reference for ECC-ozonesondes at WCCOS)
542	SHADOZ	Southern Hemisphere ADditional OZonesonde
543	SPARC	Stratosphere-troposphere Processes And their Role in Climate
544	STP	Standard Temperature (=273.15 K) and Pressure (=1013.25 hPa) conditions
545	TEI	Thermo Environmental Instruments
546	TOAR	Tropospheric Ozone Assessment Report
547	UNEP	United Nations Environment Programme
548	UTC	Universal Time Convention = Coordinated Universal Time
549	UV	Ultra-Violet
550	VMR	Volume Mixing Ratio
551	WCCOS	World Calibration Centre for OzoneSonde
552	WMO	World Meteorological Organization

553 **References**

- 554 Ancellet, A. and Ravetta, F.: Compact airborne lidar for tropospheric ozone: description and field measurements, *Appl. Opt.*,
555 37, 5509–5521, 1998.
- 556 Blot, R., Nédélec, P., Boulanger, D., Wolff, P., Sauvage, B., Cousin, J.-M., Athier, G., Zahn, A., Obersteiner, F., Scharffe, D.,
557 Petetin, H., Bennouna, Y., Clark, H., and Thouret, V.: Internal consistency of the IAGOS ozone and carbon monoxide
558 measurements for the last 25 years, *Atmos. Meas. Tech.*, 14, 3935–3951, <https://doi.org/10.5194/amt-14-3935-2021>, 2021.
- 559 Brenninkmeijer C.A.M., P.J. Crutzen, T.Z. Immelmann, D. Kersting, M. Maiss, M. Nolle, A. Pitscheider, H. Pohlkamp, D.
560 Scharffe, K. Specht, and A. Wiedensohler, CARIBIC - Civil aircraft for global measurement of trace gases and aerosols in the
561 tropopause region, *J. Atmos. Ocean. Tech.*, 16, 1373-1383, 1999.
- 562 Brenninkmeijer, C.A.M., Crutzen, P., Boumard, F., Dauer, T., Dix, B., Ebinghaus, R., Filippi, D., Fischer, H., Franke, H.,
563 Frieß, U., Heintzenberg, J., Helleis, F., Hermann, M., Kock, H. H., Koepfel, C., Lelieveld, J., Leuenberger, M., Martinsson,
564 B. G., Miemczyk, S., Moret, H. P., Nguyen, H. N., Nyfeler, P., Oram, D., O'Sullivan, D., Penkett, S., Platt, U., Pucek, M.,
565 Ramonet, M., Randa, B., Reichelt, M., Rhee, T. S., Rohwer, J., Rosenfeld, K., Scharffe, D., Schlager, H., Schumann, U., Slemr,
566 F., Sprung, D., Stock, P., Thaler, R., Valentino, F., van Velthoven, P., Waibel, A., Wandel, A., Waschitschek, K.,
567 Wiedensohler, A., Xueref-Remy, I., Zahn, A., Zech, U., and Ziereis, H.: Civil Aircraft for the regular investigation of the



- 568 atmosphere based on an instrumented container: The new CARIBIC system, *Atmos. Chem. Phys.*, 7, 4953–4976,
569 <https://doi.org/10.5194/acp-7-4953-2007>, 2007.
- 570 Brunner, D., Staehelin, J., Jeker, D., Wernli, H., and Schumann, U.: Nitrogen oxides and ozone in the tropopause region of the
571 Northern Hemisphere: Measurements from commercial aircraft in 1995/96 and 1997, *J. Geophys. Res.*, 106, 27673–27699,
572 2001.
- 573 CCQM-GAWG-2024/03: Guidelines how to implement the new absorption cross-section for ozone concentration
574 measurements, <https://www.bipm.org/documents/d/guest/rapportbipm2024-03>, 2024.
- 575 Cohen, Y., Petetin, H., Thouret, V., Marécal, V., Josse, B., Clark, H., Sauvage, B., Fontaine, A., Athier, G., Blot, R.,
576 Boulanger, D., Cousin, J.-M., and Nédélec, P.: Climatology and long-term evolution of ozone and carbon monoxide in the
577 upper troposphere–lower stratosphere (UTLS) at northern midlatitudes, as seen by IAGOS from 1995 to 2013, *Atmos.*
578 *Chem. Phys.*, 18, 5415–5453, <https://doi.org/10.5194/acp-18-5415-2018>, 2018.
- 579 Cooper, O.R., D.D. Parrish, J. Ziemke, N.V. Balashov, M. Cupeiro, I.E. Galbally, S. Gilge, L. Horowitz, N.R. Jensen, J.-F.
580 Lamarque, V. Naik, S.J. Oltmans, J. Schwab, D.T. Shindell, A.M. Thompson, V. Thouret, Y. Wang, and R.M. Zbinden:
581 Global distribution and trends of tropospheric ozone: An observation-based review. *Elementa Sci. Anthropocene*, 2, 000029,
582 doi:10.12952/journal.elementa.000029, 2014
- 583 Dias-Lalcaca, P., Brunner, D., Imfeld, W., Moser, W., and Staehelin, J.: An Automated System for the Measurement of
584 Nitrogen Oxides and Ozone Concentrations from a Passenger Aircraft: Instrumentation and First Results of the NOXAR
585 Project, *Env. Sci. Tech.*, 32, 3228–3236, 1998.
- 586 Gaudel, A., Cooper, O.R., Chang, K.-L., Bourgeois, I., Ziemke, J.R., Strode, S.A., Oman, L.D., Sellitto, P., Nédélec, P., Blot,
587 R., Thouret, V. & Granier, C.: Aircraft observations since the 1990s reveal increases of tropospheric ozone at multiple locations
588 across the Northern Hemisphere. (Vol. 6). <https://doi.org/10.1126/sciadv.aba8272>, 2020.
- 589 Petetin, H., Thouret, V., Athier, G., Blot, R., Boulanger, D., Cousin, J.-M., Gaudel, A., Nédélec, P. & Cooper, O.: Diurnal
590 cycle of ozone throughout the troposphere over Frankfurt as measured by MOZAIC-IAGOS commercial aircraft. (Vol. 4).
591 <https://doi.org/10.12952/journal.elementa.000129>, 2016.
- 592 Hearn, A.G.: Absorption of ozone in ultra-violet and visible regions of spectrum, *Proc. Phys. Soc.*, 78, 932–940, 1961.
- 593 Hodges, J.T., Viallon, J., Brewer, P.J., Drouin, B.J., Gorshchev, V., Janssen, C., Lee, S., Possolo, A., Smith, M.A.H., Walden,
594 J., Wielgosz, R.I.: Recommendation of a consensus value of the ozone absorption cross-section at 253.65 nm based on a
595 literature review, *Metrologia*. 56: 034001. <https://iopscience.iop.org/article/10.1088/1681-7575/ab0bdd>, 2019



- 596 Hu, L., Jacob, D.J., Liu, X., Zhang, Y, Zhang., L., Kim, P.S., Sulprizio, M.P., Yantosca, R.M.: Global budget of tropospheric
597 ozone: Evaluating recent model advances with satellite (OMI), aircraft (IAGOS), and ozonesonde observations, *Atm. Env.*,
598 167, 323-334, <https://doi.org/10.1016/j.atmosenv.2017.08.036>, 2017.
- 599 IPCC-Climate Change: The Physical Science Basis. Contribution of Working Group I to the Sixth Assessment Report of the
600 Intergovernmental Panel on Climate Change, edited by: Masson-Delmotte, V., Zhai, P., Pirani, A., Connors, S.L., Péan, C.,
601 Berger, S., Caud, N., Chen, Y., Goldfarb, L., Gomis, M. I., Huang, M., Leitzell, K., Lonnoy, E., Matthews, J. B. R., Maycock,
602 T. K., Waterfield, T., Yelekçi, O., Yu, R., and Zhou, B., Cambridge University Press, Cambridge, United Kingdom and New
603 York, NY, USA, in press, <https://doi.org/10.1017/9781009157896>, 2023.
- 604 Marengo, A., V. Thouret, P. Nédélec, H. Smit, M. Helten, D. Kley, F. Karcher, P. Simon, K. Law, J. Pyle, G. Poschmann, R.
605 Von Wrede, C. Hume and T. Cook: Measurement of ozone and water vapor by Airbus in-service aircraft: The MOZAIC
606 airborne program, An overview, *J. Geophys. Res.*, 103, 25,631-25,642, 1998.
- 607 McDermid, I. S., Haner, D. A., Kleiman, M. M., Walsh, T. D., and White, M. L.: Differential absorption lidar systems for
608 tropospheric and stratospheric ozone measurements, *Opt. Engin.*, 30, 22–30, 1991.
- 609 Nédélec P., Blot R., Boulanger D., Athier G., Cousin J-M., Gautron B., Petzold A., Volz-Thomas A. and Thouret V.,
610 Instrumentation on commercial aircraft for monitoring the atmospheric composition on a global scale: the IAGOS system,
611 technical overview of ozone and carbon monoxide measurements, MOZAIC-IAGOS special issue, *Tellus B* 2015, 67, 27791,
612 <http://dx.doi.org/10.3402/tellusb.v67.27791>.
- 613 Obersteiner, F.: FAIROmeta (v0.1.8), <https://doi.org/10.5281/zenodo.11104076>, 2024.
- 614 Petzold A., V. Thouret, C. Gerbig, A. Zahn, C.A.M. Brenninkmeijer, M. Gallagher, M. Hermann, M. Pontaud, H. Ziereis, D.
615 Boulanger, J. Marshall, P. Nédélec, H.G.J. Smit, U. Frieß, J.-M. Flaud, A. Wahner, J.-P. Cammas, A. Volz-Thomas, and
616 IAGOS Team: Global-Scale Atmosphere Monitoring by In-Service Aircraft - Current Achievements and Future Prospects of
617 the European Research Infrastructure IAGOS, *Tellus-B*, 67, 28452. doi:10.3402/tellusb.v67.28452, 2015.
- 618 Petzold, A., Bundke, U., Hienola, A., Laj, P., Lund Myhre, C., Vermeulen, A., Adamaki, A., Kutsch, W., Thouret, V.,
619 Boulanger, D., Fiebig, M., Stocker, M., Zhao, Z., and Asmi, A.: Opinion: New directions in atmospheric research offered by
620 research infrastructures combined with open and data-intensive science, *Atmos. Chem. Phys.*, 24, 5369–5388,
621 <https://doi.org/10.5194/acp-24-5369-2024>, 2024.
- 622 Proffitt, M.H. and McLaughlin, R.J.: Fast response dual-beam UV-absorption photometer suitable for use on stratospheric
623 balloons, *Rev. Sci. Instr.*, 54, 1719–1728, 1983.
- 624 Schnadt Poberaj, C., Staehelin, J., Brunner, D., Thouret, V., and Mohnen, V.: A UT/LS ozone climatology of the nineteen
625 seventies deduced from the GASP aircraft measurement program, *Atmos. Chem. Phys.*, 7, 5917–5936,
626 <https://doi.org/10.5194/acp-7-5917-2007>, 2007.



- 627 Schneider, M., Blumenstock, T., Hase, F., Höpfner, M., Cuevas, E., Redondas, A., and Sancho, J. M.: Ozone profiles and total
628 column amounts derived at Izana Tenerife Island, from FTIR solar absorption spectra, and its validation by an intercomparison
629 to ECC-sonde and Brewer spectrometer measurements, *J. Quant. Spectros. Radiat. Transfer*, 245-274,
630 <https://doi.org/10.1016/j.jqsrt.2004.05.067>, 2005.
- 631 Smit H.G.J., Sträter, W., Helten, M. and Kley, D.: Environmental Simulation Facility to Calibrate Airborne Ozone and
632 Humidity Sensors. Jül Berichte, No. 3796, Forschungszentrum Jülich, 2000.
- 633 Smit, H. G. J., Sträter, W., Johnson, B. J., Oltmans, S. J., Davies, J., Tarasick, D. W., Högger, B., Stübi, R., Schmidlin, F. J.,
634 Northam, T., Thompson, A. M., Witte, J. C., Boyd, I., and Posny, F.: Assessment of the performance of ECC ozonesondes
635 under quasi-flight conditions in the environmental simulation chamber: Insights from the Jülich Ozone Sonde Intercomparison
636 Experiment (JOSIE), *J. Geophys. Res.*, 112, D19306, <https://doi.org/10.1029/2006JD007308>, 2007.
- 637 Smit, H. G. J., Thompson, A. M., and the ASOPOS 2.0 Panel: Ozonesonde Measurement Principles and Best Operational
638 Practices, WMO Global Atmosphere Watch Report Series, No. 268, World Meteorological Organization, Geneva,
639 <https://library.wmo.int/idurl/4/57720> (last access: 10 December 2023), 2021.
- 640 Smit, H. G. J., Poyraz, D., Van Malderen, R., Thompson, A.M., Tarasick, D. W., Stauffer, R. M., Johnson, B. J., and Kollonige,
641 D. E.: New insights from the Jülich Ozone Sonde Intercomparison Experiment: calibration functions traceable to one ozone
642 reference instrument, *Atmos. Meas. Tech.*, 17, 73–112, <https://doi.org/10.5194/amt-17-73-2024>, 2024.
- 643 Stauffer, J., Staehelin, J., Stübi, R., Peter, T., Tummon, F., and Thouret, V.: Trajectory matching of ozonesondes and MOZAIC
644 measurements in the UTLS - Part 1: Method description and application at Payerne, Switzerland. *Atmos. Meas. Tech.*, 6, 3393-
645 3406, doi:10.5194/amt-6-3393-2013, 2013.
- 646 Stauffer, J., Staehelin, J., Stübi, R., Peter, T., Tummon, F., and Thouret, V.: Trajectory matching of ozonesondes and MOZAIC
647 measurements in the UTLS - Part 2: Application to the global ozonesonde network. *Atmos. Meas. Tech.*, 7, 241-266,
648 doi:10.5194/amt-7-241-2014, 2014.
- 649 Tarasick, D., Galbally, I.E., Cooper, O.R., Schultz, M.G., Ancellet, G., Leblanc, T., Wallington, T.J., Ziemke, J., Liu, X.,
650 Steinbacher, M., Staehelin, J., Vigouroux, C., Hannigan, J.W., García, O., Foret, G., Zanis, P., Weatherhead, E.,
651 Petropavlovskikh, I., Worden, H., Osman, M., Liu, J., Chang, K.-L., Gaudel, A., Lin, M., Granados-Muñoz, M., Thompson,
652 A.M., Oltmans, S.J., Cuesta, J., Dufour, G., Thouret, V., Hassler, B., Trickl, T. and Neu, J.L.: Tropospheric Ozone Assessment
653 Report: Tropospheric ozone from 1877 to 2016, observed levels, trends and uncertainties. *Elementa: Science of the*
654 *Anthropocene*, 7:39. <https://doi.org/10.1525/elementa.376>, 2019.
- 655 Tanimoto, H., Zbinden, R.M., Thouret, V., and Nédélec, P.: Consistency of tropospheric ozone observations made by different
656 platforms and techniques in the global databases, *Tellus B*, 67, 27073, <https://doi.org/10.3402/tellusb.v67.27073>, 2015.



- 657 Thompson, A.M., The oxidizing capacity of the earth's atmosphere: Probably past and future changes, *Science*, 256, 1157-
658 1165, 1992.
- 659 Thouret, V., A. Marenco, J. A. Logan, P. Nédélec, and C. Grouhel, Comparisons of ozone measurements from the MOZAIC
660 airborne program and the ozone sounding network at eight locations, *J. Geophys. Res.*, 103, 25,695-25,720, 1998.
- 661 Vigouroux, C., De Mazière, M., Demoulin, P., Servais, C., Hase, F., Blumenstock, T., Kramer, I., Schneider, M., Mellqvist,
662 J., Strandberg, A., Velasco, V., Notholt, J., Sussmann, R., Stremme, W., Rockmann, A., Gardiner, T., Coleman, M., and
663 Woods, P.: Evaluation of tropospheric and stratospheric ozone trends over Western Europe from ground-based FTIR network
664 observations, *Atmos. Chem. Phys.*, 8, 6865–6886, <https://doi.org/10.5194/acp-8-6865-2008>, 2008.
- 665 Wagner, A., Bennouna, Y., Blechschmidt, A.-M., Brasseur, G., Chabrillat, S., Christophe, Y., Errera, Q., Eskes, H., Flemming,
666 J., Hansen, K.M., Inness, A., Kapsomenakis, J., Langerock, B., Richter, A., Sudarchikova, N., Thouret, V. & Zerefos, C.
667 (2021). Comprehensive evaluation of the Copernicus Atmosphere Monitoring Service (CAMS) reanalysis against independent
668 observations. (Vol. 9). <https://doi.org/10.1525/elementa.2020.00171>
- 669 Wang, H., Lu, X., Jacob, D.J., Cooper, O.R., Chang, K.-L., Li, K., Gao, M., Liu, Y., Sheng, B., Wu, K., Wu, T., Zhang, J.,
670 Sauvage, B., Nédélec, P., Blot, R. & Fan, S. (2022). Global tropospheric ozone trends, attributions, and radiative impacts in
671 1995–2017: an integrated analysis using aircraft (IAGOS) observations, ozonesonde, and multi-decadal chemical model
672 simulations. (Vol. 22, pp. 13753-13782). <https://doi.org/10.5194/acp-22-13753-2022>
- 673 Wang, H., Tarasick, D.W., Liu, J., Smit, H.G.J., Van Malderen, R., Shen, L., Blot, R., and Zhao, T.: Consistency evaluation
674 of tropospheric ozone from ozonesonde and IAGOS (In-service Aircraft for a Global Observing System) observations: vertical
675 distribution, ozonesonde types, and station–airport distance, *Atmos. Chem. Phys.*, 24, 11927–11942,
676 <https://doi.org/10.5194/acp-24-11927-2024>, 2024.
- 677 Wilson, K.L. and Birks, J.W.: Mechanism and Elimination of a Water Vapor Interference in the Measurement of Ozone by
678 UV Absorbance, *Env. Sci. Tech.*, 40 (20), 6361–6367, DOI: 10.1021/es052590c, 2006.
- 679 WMO/UNEP: Scientific Assessment of Ozone Depletion: 2022, Ozone Research and Monitoring, GAW Report No. 278,
680 World Meteorological Organization, Geneva, ISBN: 978-9914-733-97-6, <https://library.wmo.int/idurl/4/58360> (last access: 10
681 December 2023), 2023.
- 682 Zahn, A.: Standard Operating Procedure (SOP) of the IAGOS-CARIBIC Ozone Instrument, IAGOS-Technical Document,
683 2016.
- 684